Atmospheric Environment 356 (2025) 121305

Contents lists available at ScienceDirect

Atmospheric Environment

journal homepage: www.elsevier.com/locate/atmosenv

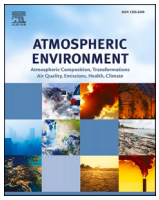

A model-based estimate for the direct radiative effect of atmospheric microplastics

Qiaotong Pang [a], Xuan Wang [b], Bingliang Zhuang [a], Haikun Wang [a], Yanxu Zhang [c,*]

[a] School of Atmospheric Sciences, Nanjing University, Nanjing, Jiangsu, 210023, China
[b] School of Energy and Environment, City University of Hong Kong, Hong Kong, China
[c] Department of Earth and Environmental Sciences, Tulane University, New Orleans, 70118, USA

HIGHLIGHTS

- Integrate an atmospheric microplastics (MPs) model and a radiative transfer model.
- Quantify the Direct Radiative Effects (DRE) of MPs.
- Reveal the spatial distribution pattern of MPs' DRE.
- Identity main affected-areas and critical factors of MPs' DRE.

ARTICLE INFO

Keywords:
Atmospheric microplastics (MPs)
Direct radiative effects (DRE)
Atmospheric flux
Cooling effects

ABSTRACT

Atmospheric microplastics (MPs) have emerged as novel atmospheric pollutants, with the potential to impact ecosystems and human societies in numerous ways. As aerosols, MPs can both absorb and scatter radiation, influencing atmospheric flux and possibly contributing to global climate change. In this study, we quantify the direct radiative effects (difference of atmospheric flux with and without MPs) (DREs) of MPs by integrating an atmospheric transport and radiative transfer model. The results reveal a global annual mean shortwave radiation DRE of −9.07 (−40.57–2.04) μW m^{-2} and a longwave radiation DRE of +2.73 (0.61–12.21) μW m^{-2}. Our findings suggest that the total DRE of MPs is concentrated in densely populated and arid regions, driven by high emission rates and favorable atmospheric conditions. The contribution of ocean sources to the DRE is relatively low compared to land-based sources. We find that MPs exert stronger radiative effects at the top of the atmosphere, comparing to at the Earth's surface, as the magnitude of net DRE decreases from −6.34 (−28.36–1.43) μW m^{-2}o −1.93 (−8.68–0.44) μW m^{-2}. Additionally, the DRE is size-dependent, with larger effect as MP size increases. As plastic pollution continues to rise, the contribution of MPs to radiative effect and climate change is expected to grow. We emphasize the urgent need for early actions to control atmospheric MPs to mitigate potentially severe climate impacts.

1. Introduction

Plastics have become an indispensable part of modern life, indicating the onset of a plastic age. In 2021, the global plastic production reached 391 million metric tons (Global plastic production share by region 2023, 2024), far surpassing the world crude steel production in the same year if compared in volume (World Steel in Figures 2022 - Worldsteel. Org, 2023). However, mismanaged plastic waste has emerged as a significant environmental contaminant, including in the atmosphere, due to its durability, ubiquity, and potential impact on the climate, ecosystem, and human health (Allen et al., 2022; Fu et al., 2023; Luo et al., 2024; Revell et al., 2021). Among these, microplastics (MPs) and nanoplastics (NPs) with sizes of 1–5000 μm and < 1um, respectively, resulting from the fragmentation of larger plastic debris, are of particular concern due to its long residence times and transport potential in the environment (Chen et al., 2023; Cózar et al., 2014; Evangeliou et al., 2020). Here we focus on the direct radiative effect (DRE) of atmospheric MPs.

The radiative effect of MPs depends on their optical properties and atmospheric abundance (Revell et al., 2021). Owing to their good optical characteristics, microplastics are composed of synthetic polymers,

* Corresponding author.
E-mail address: yzhang127@tulane.edu (Y. Zhang).

https://doi.org/10.1016/j.atmosenv.2025.121305
Received 12 February 2025; Received in revised form 14 May 2025; Accepted 16 May 2025
Available online 17 May 2025

which have been widely used in aerospace, optical lens, electronics, and solar cells (Zhang et al., 2020). Studies for the radiative effects of atmospheric MPs remain rare and cannot cover all types of polymers, however, few experimental studies on the scattering cross-sections of non-pigment fragments and fibers indicate that MPs are efficient at scattering ultraviolet and visible radiation, which has a cooling effect on surface climate (Revell et al., 2021). Meanwhile, they can absorb infrared radiation, especially at the 'atmospheric window' (8–12 μm) where the atmosphere is relatively transparent, contributing the greenhouse effect (Revell et al., 2021). There is large spatiotemporal variability in the atmospheric abundance of MPs (Allen et al., 2022). As an initial effort, Revell et al. (2021) estimated the net directive radiative effect (net DRE) of MP as 0.044 ± 0.399 mW m^{-2} by assuming a uniform MP concentration of 1 items m^{-3} in the surface and an exponential decrease vertical profile. Confining MP in the boundary layer changes the net DRE to -0.746 ± 0.553 mW m^{-2} (Revell et al., 2021). Yang et al. (2024) also calculate the net DRE of MPs to be between −30 and 30 mW m^{-2} at the top of atmosphere and −90 to 720 mW m^{-2} at the Earth's surface by using much higher MP concentrations (200–464 items m^{-3}) observed in a megacity in the North China Plain.

Atmospheric MPs have been extensively monitored around the world in recent years, as summarized by Allen et al. (2022) and Fu et al. (2023). Three types of data exist in the literature: air concentration, deposition, and surface sampling data, which measure the MP concentrations in surface air (including land and ocean), falling flux to the ground, and accumulation at the surface such as road dust/snow, and ice, respectively. These data indicate a relatively low concentrations of MPs (<10 items m^{-3}) in the marine boundary layer but are potentially relatively high at terrestrial and urban sites (approximately 100-1000 but up to 1000–10,000 items m^{-3}). The MP deposition fluxes often range from 10 to 100 items m^{-2} per day in remote areas but can be elevated to 1000–10,000 items m^{-2} per day in urban areas or regions subjected to long range transport. These variabilities are caused not only by spatiotemporal variations in its emissions and transport, but also by the non-standardized analytical methods used in this study (Fu et al., 2023). The surface sampling data vary even more drastically depending on the type of sample media and its representative time scale for MP accumulation (Chen et al., 2023; Yang et al., 2024).

Here, we calculate the DRE of atmospheric MPs by employing atmospheric MP concentrations derived from Bayesian inference and data assimilation techniques (Brahney et al., 2021; Fu et al., 2023; Long et al., 2022). These studies developed atmospheric MP transport models at regional or global scales (e.g., CAM5, WRF-MP, and GC-MP). With hypothesized emission sources (e.g., road dust, ocean spray, and agricultural dust), they derived best estimated emissions by minimizing the model-observation difference (i.e., optimal estimation method). They adopted observations for the atmospheric MP deposition flux over the western United States or suspended MP concentrations over Asia and adjacent oceans (Brahney et al., 2021; Long et al., 2022). Fu et al. (2023) developed the GC-MP model and achieved a global coverage by using all available suspended MP concentration and deposition flux data worldwide. They suggested global atmospheric MP emissions of 324 (73–1450) Gg $year^{-1}$. We employ the atmospheric MP concentrations simulated by the GC-MP model and estimate the DRE by using the rapid radiative transfer model for general circulation models (RRTMG), which is offlinely coupled with the GC-MP and standard GEOS-Chem full chemistry models with optical properties following Revell et al. (2021). Our objectives are to: i) estimate the DRE of MPs by quantifying their impacts on shortwave and longwave radiation; ii) analyze the spatial patterns of DRE to identify key regions where MPs contribute significantly to radiative flux; iii) evaluate the contributions of MPs of different sizes and sources to DRE.

2. Method

2.1. Atmospheric microplastic simulation

We simulate both the vertical and horizontal distributions of MPs in the atmosphere via the GEOS-Chem-Microplastic (GC-MP) model (Fu et al., 2023). The GC-MP model is based on the global three-dimensional GEOS-Chem model version 14.1.1 (https://wiki.seas.harvard.edu/geos-chem/index.php/GEOS-Chem_14.1.1), with a horizontal resolution of 0.5° latitude × 0.625° longitude and 72 vertical layers extending to 0.01 hPa. The emission, transport and deposition of MPs with six different aerodynamic diameters size bin (0.3, 2.5, 7, 15, 35, and 70 μm) are simulated in the GC-MP model, following the methodology of Brahney et al. (2021). Spherical shapes of all MPs are used in this model for simplicity. The residence time of MPs ranges from 0.04 to 6.5 days depending on their aerodynamic dimeters. The transport of MPs in this model is computed by adapting the TPCORE advection algorithm (Lin and B. Rood, 1996) and the convective transport method comes from Wu (2004). Multiple deposition processes of MPs are incorporated into the GC-MP model, including wet deposition, scavenging of aerosols by snow and cold/mixed precipitation, dry deposition, and gravitational deposition (Alexander et al., 2005; Duncan Fairlie et al., 2007; Jaeglé et al., 2011; Liu et al., 2001; Q. Wang et al., 2011; Wu, 2004). Meteorological data from the GEOS are used in this model (https://gmao.gsfc.nasa.gov/GMAO_products/NRT_products.php). We run this model from 2018 to 2020, and the simulated distributions of MPs (as depicted in Fig. 1) are used to further estimate the DRE of MPs.

2.2. MP emission sources

Emissions of MPs from various sources, including aerosolized marine plastic, traffic-related sources, resuspension of mismanaged plastic wastes (MMPW) and agricultural plastic waste, and generic sources associated with residential activities are considered in this model. However, the contributions from each source to atmospheric MPs emission are generally unclear due to the lack of comprehensive atmospheric emission inventories. To estimate the magnitudes of the five MPs emission sources mentioned above, Fu et al. (2023) adapted an optimal estimation method based on simulation results and observation data, compiling an atmospheric MPs inventory (Brahney et al., 2021; Long et al., 2022). The optimized atmospheric MPs emission is 324 Gg $year^{-1}$, with a 95 % confidence interval (CI) ranging from 73 to 1450 Gg $year^{-1}$. The ocean sources represent the largest emission source (171 Gg $year^{-1}$), followed by the terrestrial sources (154 Gg $year^{-1}$), the road sources (115 Gg $year^{-1}$), the agricultural sources (38 Gg $year^{-1}$), the residential sources (0.8 Gg $year^{-1}$), and the MMPW Residential sources (0.11 Gg $year^{-1}$).

2.3. Atmospheric aerosols

We also run a standard full chemistry simulation of GEOS-Chem 14.11 to simulate other aerosol tracers contemporaneous with MPs in the atmosphere. The simulation resolution for these aerosols is 4° × 5° horizontally and 72 levels vertically. We further input aerosols such as the sulfate aerosols, aerosol ammonium salts, black carbon, and dust into the direct radiative effect calculation. These concentrations are also linear interpolated to the same resolution as the atmospheric MP concentrations.

2.4. Direct radiative effect calculation

We use the RRTMG model to calculate the DRE of atmospheric MPs (Clough et al., 2005; Heald et al., 2014). The RRTMG model is a rapid radiative transfer model that uses the correlated-k approach to calculate fluxes and heating rates both efficiently and accurately. We also treat the MPs in the RRTMG as spherical shapes in consistence with the

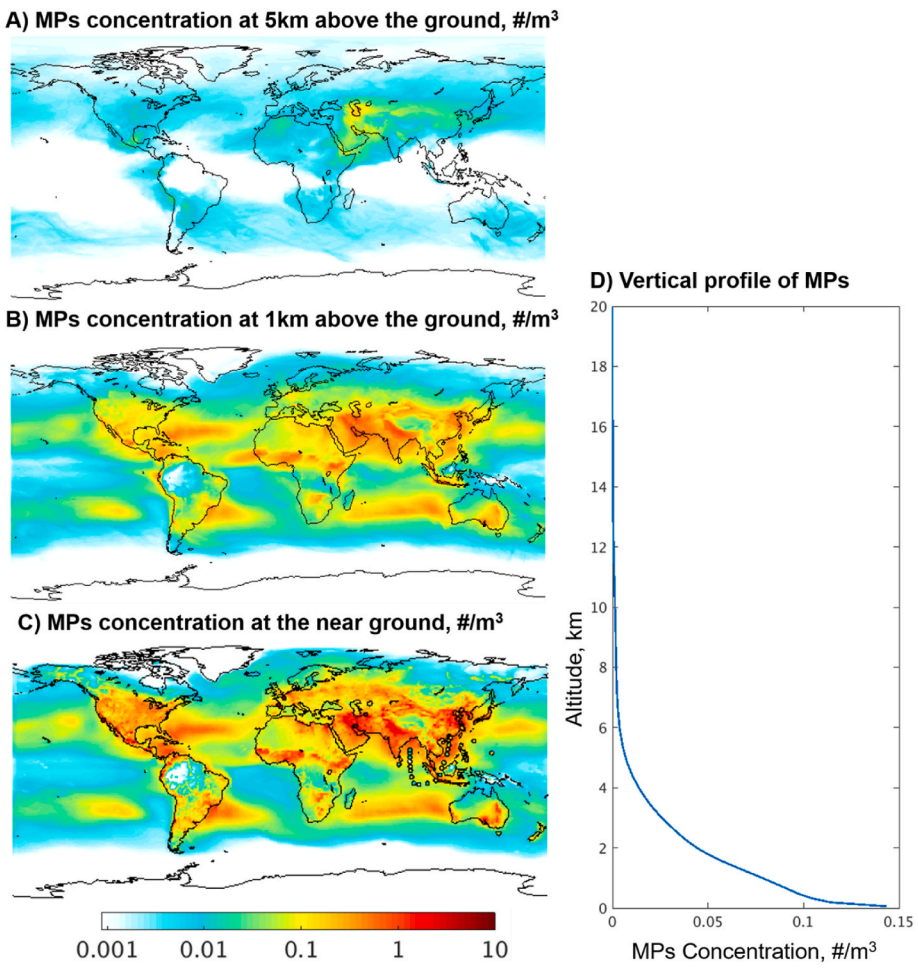

Fig. 1. Annual average atmospheric concentrations of MPs A) at 5 km above the ground, B) at 1 km above the ground, and C) at the near ground [the circles represent observation data summarized by Allen et al. (2022) from observation studies]; D) Vertical profile of atmospheric MPs concentrations.

atmospheric MP simulation. With GEOS-Chem simulated aerosol mass, we calculate optical properties including aerosol optical depth (AOD), single scattering albedo (SSA) and asymmetry factor (ASY) for MPs based on the refractive indices of pure polymers of MPs following Revell et al. (2021) and other aerosols (sulfate aerosols, nitrate aerosols, dust and others based on Wang et al. (2024)). The surface albedo is based on the multi-wavelength land composites from MODIS with 0.05 × 0.05° horizontal resolution (Heald et al., 2014; Schaaf et al., 2002). The color of atmospheric MPs is not included in our simulation and calculation as they are assumed to be non-pigmented in Revell et al. (2021)'s optical property measurement experiment. The RRTMG model considers 16 bands of wavelengths at longwave and 13 bands of wavelength at shortwave as shown in Table S1 and Table S2.

These optical properties are used as inputs for RRTMG, along with other information from GEOS-Chem (Heald et al., 2014), to derive radiative fluxes. The longwave and shortwave DRE of MPs (DRE_{SW} and DRE_{LW}) are calculated as the differences between the total flux and the flux without MPs:

$$DRE_{SW/LW} = Radiative\_fluxes_{SW/LW(withMPs)} - Radiative\_fluxes_{SW/LW_{(withoutMPs)}} \quad (1)$$

where $Radiative\_fluxes_{SW/LW(withMPs)}$ and $Radiative\_fluxes_{SW/LW(wioutMPs)}$ represent the radiative fluxes with and without MPs calculated by the RRTMG. The net DRE (DRE_{net}) can be further calculated as:

$$DRE_{net} = DRE_{SW} + DRE_{LW} \quad (2)$$

We also calculate the contribution of MPs from different emission sources and with different size bins to DRE by separating $DRE_{SW/LW}$ with emission source (*src*) and size bins (*bin*):

$$DRE_{SW/LW(src(n))} = Atmospheric\_fluxes_{SW/LW(src(n))} - Atmospheric\_fluxes_{SW/LW(withoutMPs)} \quad (3)$$

$$DRE_{SW/LW(bin(m))} = Atmospheric\_fluxes_{SW/LW(bin(m))} - Atmospheric\_fluxes_{SW/LW(withoutMPs)} \quad (4)$$

where *src*(n) with $n = 1$ to 5 represents atmospheric MPs from the ocean sources, the MMPW sources, the agricultural sources, the residential sources, and the road sources, respectively; *bin*(m) with m = 1 to 6 represents atmospheric MPs with a **radius** of 0.3 μm, 2.5 μm, 7 μm, 15 μm, 35 μm, and 70 μm, respectively. A Gamma distribution was adopted to calculate the radiative effects of atmospheric MPs based on a wavelength-dependent refractive index. Both the size distribution and optical properties included in the model followed (Revell et al., 2021), in which they are reflective of observations.

3. Results and discussion

3.1. Atmospheric MPs distribution

Our simulation reveals uneven distributions of atmospheric MPs both horizontally and vertically as depicted in Fig. 1. The abundance of atmospheric MPs in terrestrial regions is generally linked to human activities. Coastal areas such as East Asia and major river deltas like the

Ganges Delta exhibit significantly elevated concentrations of MPs, with notable hotspots near densely populated areas. Regions like northern India and the coasts of the Persian Gulf show particularly high MP concentrations, exceeding 10 items m^{-3} near the ground (Fig. 1C). These regions are characterized by substantial human activity and inadequate waste management infrastructure, leading to increased emissions of plastic debris into the environment. Atmospheric MPs suspended over the oceanic regions are influenced not only by the long-range transport of plastic pollution from densely populated land areas, such as Southeast Asia, but also by the abundant stock of oceanic plastics, such as the Great Garbage Patch in both hemispheres as depicted in Fig. 1C. In contrast, remote regions far from urban centers, such as the Amazon rainforest, the Sahara Desert, and the polar regions, have much lower MP concentrations, reflecting reduced input sources and limited long-distance transport of MPs in the atmosphere (Fu et al., 2023). Coastal and near-shore oceanic regions also display moderate atmospheric MPs concentrations, likely influenced by deposition from ocean-sourced MPs and proximity to human activity. Our modeling results indicate that the global annual average concentration of atmospheric MPs near the ground is 0.14 items m^{-3} as shown in Fig. 1D. Due to the different ranges of observation data used in models, our estimation of atmospheric MPs concentrations is lower than Evangeliou et al. (2022) (1–8 items m^{-3}), but close to Long et al. (2022) (0.024–0.39 items m^{-3}). Our modeling results for atmospheric MPs concentrations is still robust, with root-mean-squared errors (RMSE) between logarithm-transformed modeling results and observations of 0.65 and 0.37 order of magnitude for atmospheric concentrations and depositions, respectively (Fu et al., 2023). Moreover, some studies report higher observed concentration of atmospheric MPs of 100s and even 1000s items m^{-3} in megacities (Zhu et al., 2021), these high measurement values cannot represent regional mean condition of atmospheric MPs distribution. Our study is focusing on global and region DRE of atmospheric MPs, rather than resolving the local influence of DRE from atmospheric MPs.

The concentration of atmospheric MPs decreases exponentially from the near ground to the top of atmosphere (Fig. 1A, B, and 1D). Due to gravitational settling, most airborne MPs remain below an altitude of 20 km. The global annual average concentration of atmospheric MPs near the ground is 0.14 items m^{-3}, but it decreases by 50 % at 1 km above the ground and further drops to 0.005 items m^{-3} at 5 km. This pattern reflects the limited vertical transport of MPs. The model simulates fewer MPs at higher altitudes over the ocean compared to land (Fig. 1A & B). Despite the significant decrease in MPs concentration in most densely populated regions worldwide at altitude above 5 km, substantial concentrations still accumulate over the Middle East region. Notably, the maximum MPs concentration in this area is simulated to be 0.24 items m^{-3} (Fig. 1A).

We also simulate the concentrations of atmospheric MPs with different sizes (Fig. 2). The mid-sized MPs (7 μm, 15 μm and 35 μm) account for more than 85 % of total MPs near the ground. The spatial distribution of MPs also depends on the particle sizes. These particles are primarily emitted from anthropogenic sources, such as industrial activity, road transport, and agricultural practices (Yang et al., 2024), leading to regional hotspots in East Asia, Europe, and North America. In contrast, smaller particles (e.g., 0.3 μm and 2.5 μm) exhibit a more uniform distribution, reflecting their ability to be transported over longer distances. Larger particles (e.g., 70 μm) remain concentrated near their sources, with limited spatial dispersion due to relatively rapid gravitational settling.

3.2. DRE of atmospheric MPs

We calculate the radiative effect of atmospheric MPs by running the RRTMG model with the simulation results from the GC-MP model. The RRTMG model calculates a global mean radiative effect of −9.07 and + 2.73 μW m^{-2} for shortwave and longwave radiation, respectively, with a net DRE of −6.34 μW m^{-2} at the top of atmosphere, as shown in Fig. 3. This indicates cooling and warming effects of MPs at the top of atmosphere for shortwave and longwave wavelengths, respectively. We also calculate the net DRE of atmospheric MPs at the Earth's surface, which is −1.93 mW m^{-2}. The net DRE of atmospheric MPs is lower than the estimate of Revell et al. (2021), 44 μW m^{-2}, due to lower atmospheric MP abundance modeled from our GC-MP simulation used. Indeed, Revell et al. (2021) assumed a uniform concentration of the atmospheric MPs as 1 items m^{-3} based on limited observation data, which were mainly obtained in densely populated areas, ignoring remote areas with sparse human activities. Furthermore, they only considered atmospheric concentration measurements. In contrast, GC-MP model integrates both atmospheric concentration and the deposition data for MPs and improve the simulation results by using an optimal estimation method (Fu et al., 2023). As a result, our simulated spatial distribution and concentrations of MP are potentially more accurate, with varying concentrations in different locations within the atmosphere.

The model also suggests significant spatial variability, with the highest annual mean DRE of −465 μW m^{-2} for shortwave radiation (referred as DRE_{SW}) and 85.6 μW m^{-2} for longwave radiation (hereafter referred as DRE_{LW}) in regions such as the Middle East, North India, and East Asia. The annual mean DRE of atmosphere MPs for shortwave radiation follows a similar spatial pattern to that of MPs distribution as shown in Fig. 1. For shortwave radiation, atmospheric MPs exhibit significant negative radiative effect in regions with high plastic abundance,

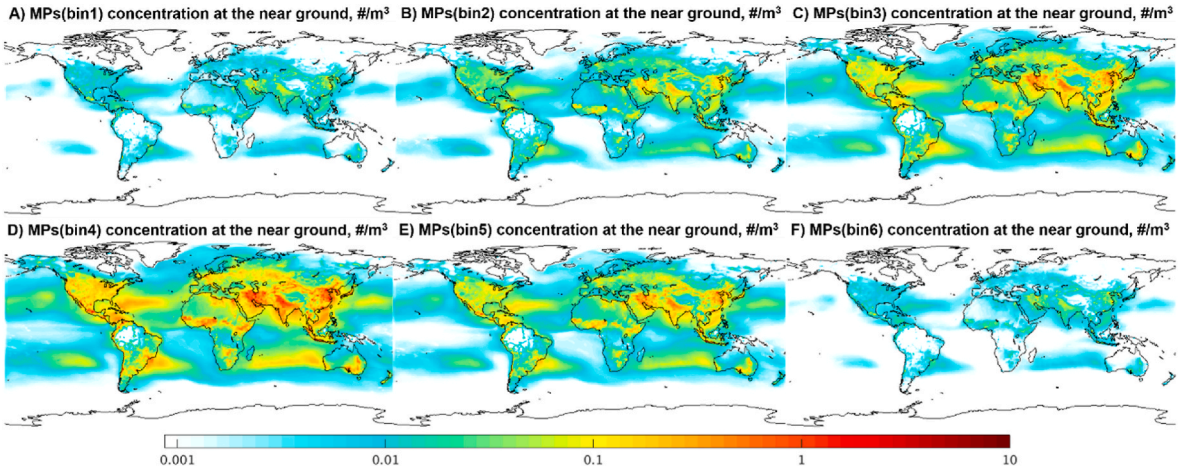

Fig. 2. Annual average concentration of the atmospheric concentration of MPs with different sizes: A) bin1 (0.3 μm), B) bin2 (2.5 μm), C) bin3 (7 μm), D) bin4 (15 μm), E) bin5 (35 μm), F) bin6 (70 μm).

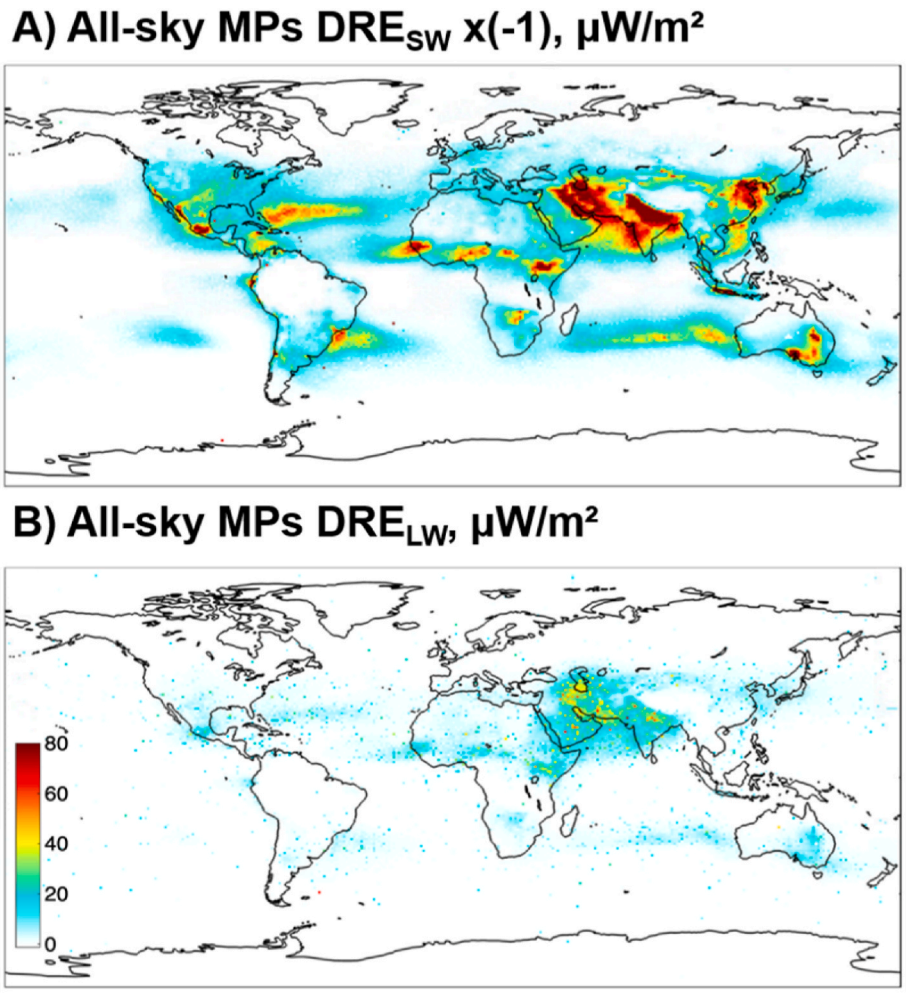

Fig. 3. Annual mean all-sky MPs DRE at the top of atmosphere. A) DRE_{SW}; B) DRE_{LW}. Please note the DRE_{SW} is plotted in an opposite sign to use the same scale with DRE_{LW}.

particularly over East Asia, South Asia, the Middle East, and parts of Africa (Fig. 3A). These areas are hotspots for plastic pollution due to thriving human activities and common waste mismanagements, which lead to significant atmospheric plastic emissions. The negative radiative effect (nearly lower than −400 μW m^{-2}) of atmospheric MPs for shortwave radiation, modeled in these regions, suggests that MPs may contribute to localized atmospheric cooling. For instance, Yang et al. (2024) also calculates a negative DRE of −30,000 μW m^{-2} in a megacity in the East Asia with high atmospheric MPs concentration (with detected atmospheric MPs there ranging from 200 to 464 items m^{-3}).

The radiative effect caused by atmospheric MPs for longwave appears milder, with the annual mean DRE in most areas being less than 40 μW m^{-2}, as depicted in Fig. 3B. For longwave radiation, MPs in the atmosphere absorb infrared radiation and re-emit it, partially back toward the surface, creating a heat-trapping effect like greenhouse gases. The highest DRE_{LW} is primarily simulated over the Middle East, where surface temperature is high, and drought conditions prevail. In areas with high water vapor content, the dominance of water vapor absorption can overshadow the DRE_{LW} of MPs, making their contribution relatively smaller. However, arid regions allow MPs to have more pronounced radiative effect. Additionally, the warming effect of MPs may be enhanced in these regions, as MPs lifetimes can be extended due to low precipitation. In contrast, regions with low plastic concentrations, such as the Southern Hemisphere and polar areas, exhibit minimal longwave effects. While the DRE_{LW} of MPs is generally weaker than their DRE_{SW}, it remains a critical component of the overall climate impact of MPs. This spatial contrast further underscores the role of human activities and proximity to source regions in driving the radiative impact of MPs under radiation.

To further investigate the spatial distribution of the atmospheric MPs DRE, we compare the DRE of MPs over the ocean and land. We observe notable differences in their impact on DRE_{SW} and DRE_{LW}. Specifically, as shown in Fig. 3A and B, the DRE of MPs over the ocean is considerably smaller than over land, with the effects being less pronounced on the ocean surface. For instance, the annual mean DRE_{SW} and DRE_{LW} of MPs at the top of the atmosphere over land are −14 μW m^{-2} and 4.5 μW m^{-2}, respectively, whereas over the ocean, DRE_{SW} and DRE_{LW} are −7.1 μW m^{-2} and 2.0 μW m^{-2}, respectively. This reflects higher atmospheric MP concentrations over the land. Even though the total oceanic sources (170.5 Gg/yr) are slightly larger than the terrestrial sources (153.5 Gg/yr) (Fu et al., 2023), but the atmospheric MP concentrations are lower over the ocean due to the larger surface area and faster deposition of coarse aerosols. Such disparity may be explained by the lower surface albedo of the ocean than of the land (Heald et al., 2014). This difference in radiative effect results in a greater net DRE over land than over the ocean. Specifically, the net DRE on land is −9.5 μW m^{-2}, which is larger than the ocean's value of −6.34 μW m^{-2}. These findings suggest that terrestrial MP exert a more pronounced impact on altering the energy balance, potentially leading to more significant local and regional climate variations compared to MP over the ocean.

3.3. Uncertainties of DRE

One of the primary sources of uncertainty in the calculated DRE arises from the estimation of the total mass of atmospheric MPs, which is based on the GC-MP model. The GC-MP model adapts inverse modeling techniques to optimize the MP emission and subsequently the atmospheric MP abundance (Fu et al., 2023). Inverse modeling involves using observed data to infer the total emissions of MP from atmospheric MP concentrations and deposition measurements. However, this approach relies on several assumptions about the initial distribution, atmospheric transport, and deposition rates of MPs, which could introduce uncertainties. The uncertainty in the total mass estimate is further compounded by limited observational data, especially for remote or oceanic regions. As a result, variations in the total mass of MPs could lead to discrepancies in the calculated DRE. Revell et al. (2021) estimate the net global mean TOA radiative effect of atmospheric MPs to be −746 μW/m^2, assuming a global atmospheric MPs concentration of 1 items m^{-3}. Yang et al. (2024) report a much higher value of −30,000 μW m^{-2} based on a higher concentration of atmospheric MP of 464 items m^{-3}. In our study, the optimized annual emissions of the atmospheric MPs are 324 Gg year^{-1}, ranging from 73 to 1450 Gg year^{-1} as the 95 % CI. Corresponding global average and maximum atmospheric MPs concentrations are 0.14 items m^{-3} (95 % CI: 0.03 to 0.63 items m^{-3}) and 19 items m^{-3} (95 % CI: 4.28 to 85.03 items m^{-3}), respectively. We calculate MPs' DRE under different emission scenario as shown in Fig. 4, finding annual mean DRE$_{SW}$ and DRE$_{LW}$ of −40.57 to −2.04 μW m^{-2} and 0.61–12.21 μW m^{-2} at the top of the atmosphere. However, these ranges of DRE may not be sufficient to describe the uncertainties from the estimate of the atmospheric MPs mass as much higher emissions are reported in other studies, such as nearly 10,000 Gg year^{-1} reported by Yang et al. (2025) and 8738 Gg year^{-1} reported by Brahney et al. (2021). Due to the resolution limitation of our model, our study is also limited to reflect the potential significant enhanced DRE in high plastic polluted urban areas such as that reported by Yang et al. (2024). Future efforts to refine inverse modeling methods, along with more precise data on MP emissions and atmospheric concentrations, will help reduce this uncertainty. Meanwhile, understanding the transport and radiative behavior of MPs from different sources is also crucial for accurately assessing their environmental impacts.

The size distribution of atmospheric MPs is a significant source of uncertainty. In our study, we focused on three size bins: 15 μm, 35 μm, and 70 μm, based on their prevalence in atmospheric MP samples. However, the true size distribution of MPs in the atmosphere is not well understood, particularly for particles smaller than 0.7 μm or larger than 70 μm. While our study suggests that MPs of 35 μm and 70 μm contribute the most to radiative effect, uncertainties in the distribution of smaller or larger particles may influence the DRE results. Smaller particles (less than 0.7 μm) may be underrepresented in our study due to their lower atmospheric concentrations. The Gamma size distribution used in our study may underestimate atmospheric MPs with smaller size as recent observation suggests that smaller MPs are more abundant than larger MPs (Morioka et al., 2024). Meanwhile, their ability to transport long distances, and influence cloud formation is still uncertain. Larger MPs (>70 μm) could interact with radiation differently, especially in terms of scattering and absorption efficiency, and may contribute differently to radiative effect than our model predicts. Therefore, a better understanding of the global size distribution of atmospheric MPs, particularly for extremes in particle sizes **and their representation in atmospheric models** are needed to reduce uncertainties in DRE calculations.

The shape of MPs is another factor that could influence their radiative effects. Microplastics can exist in a variety of shapes, including spheres, fibers, and irregular fragments. While shape can affect the scattering and absorption properties of the particles. previous studies have found for other aerosols, irregulate shape usually make extinction larger than pure sphere, so our estimates are likely to be at the lower bound (Huang et al., 2023). In this study, we assumed a spherical shape for simplicity, which is a common assumption in radiative transfer models for aerosols. However, more detailed studies of the optical properties of different microplastic shapes could refine this assumption and provide more accurate estimates of their radiative effects. Although shape is likely not the most significant source of uncertainty in this study, further research on the variation in particle morphology may help improve future radiative effect models.

The color of MPs is also likely an important factor that influences their DRE but remains uncertain. The color of MP influences their absorption and scattering properties, as dark-colored particles tend to absorb more radiation, while lighter-colored particles scatter more. However, we cannot fully account for this factor in our model due to the lack of available data on the color distribution of MPs in the atmosphere. In addition, there is also knowledge gap in the absorption and scatter

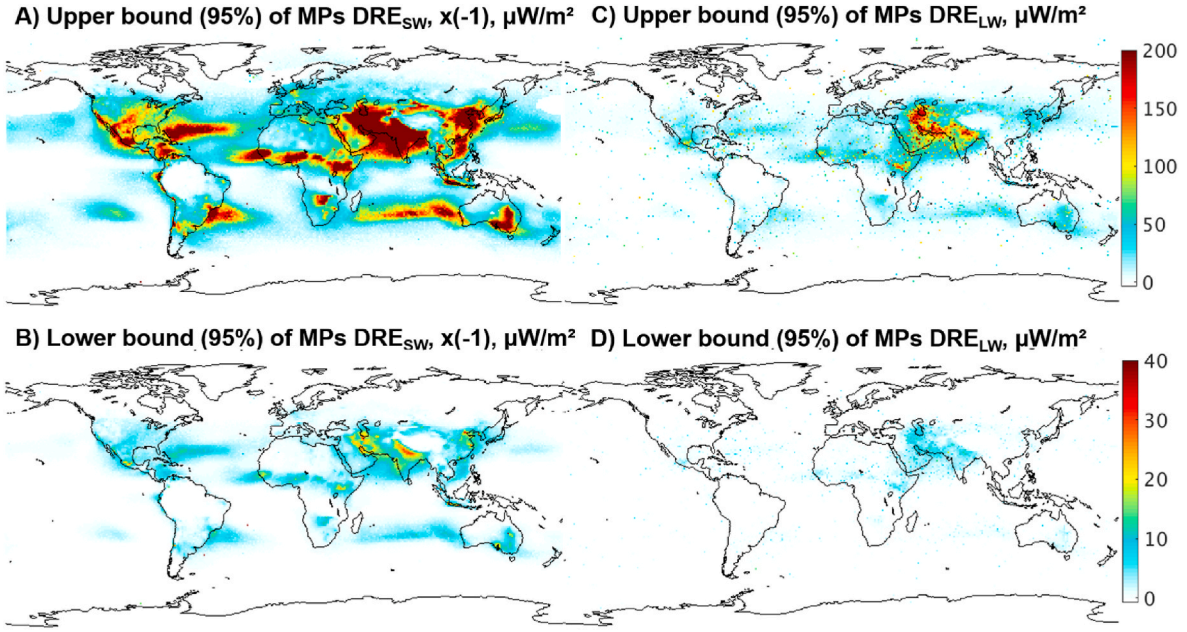

Fig. 4. Annual mean DRE$_{SW}$ and DRE$_{LW}$ of MPs at top of atmosphere under maximum emission A) and C); under minimum emission B) and D).

coefficients of MP in different colors. Under the effect of photochemical aging by UV radiation and oxidants (Leresche et al., 2021), atmospheric MPs with different initial colors may gradually fade or even become non-pigmented, which has similar optical properties as measured in Revell et al. (2021). However, the aging process of MPs may also result in browning and increased radiation absorption (Xu et al., 2024). Moreover, initial colors of MPs also play key roles in its photochemical aging (Zhao et al., 2022). Therefore, the impact of color on the radiative effects of MPs remains speculative. However, as research on the optical properties of MPs advances, we will be able to integrate effects of color and aging on atmospheric MPs optical properties into future models to improve the accuracy of DRE estimates.

3.4. Plastic emission sources' contribution to DRE

We calculate the DRE of MPs at the top of atmosphere from different emission sources. Given the uncertainty of our estimate for individual sources, we use the middle values to calculate these contributions, but the contributions from the high and low scenarios can be calculated by a similar approach. As illustrated in Fig. 5A, B and 5C, the contributions from the ocean, agriculture, and road to the total DRE_{SW} are 29 %, 25 %, and 46 %, respectively. However, these three sources' contribution to atmospheric MPs emission are 52 %, 12 %, and 35 %, respectively. Such difference can be explained by the higher surface albedo in areas with developed road networks and regions with intensive agriculture activities compared to the ocean. The contribution to DRE from the same atmospheric MPs emission source also varies with different wavelength as the contribution proportion of these three sources to DRE_{LW} are 17 %, 33 % and 50 %, respectively. Such difference is most significant for ocean-sourced MPs as ocean-sourced MPs is more dispersed at higher altitudes, which may reduce their exposure to strong long-wave radiation from the surface and the atmosphere. Meanwhile, the lower contribution of DRE_{LW} from ocean-sourced MPs comparing to DRE_{SW} can also be explained by the stronger overshadow of water vapor above the ocean. The contribution of these emission sources to the net DRE is similar to their contributions to DRE_{SW}, at 34 %, 21 % and 45 %, respectively. In contrast, the contribution from residential sources and the MMPW sources exert minimal influence on both DRE_{SW} and DRE_{LW}, as illustrated in Fig. S1. DRE_{LW} from ocean, agricultural, and road-sourced MPs all show similar spatial patterns to DRE_{SW}, with the same regions exhibiting the strongest impacts as shown in Fig. 5C, D and 5E.

Different sources of MPs exhibit varied spatial distribution patterns in their associated DRE. The spatial pattern of DRE_{SW} from ocean-sourced MPs (Fig. 5A) mirrors the distribution of oceanic plastic pollution, as described by Zhang et al. (2023). The radiative effect caused by ocean-sourced MPs is particularly concentrated in the coastal waters along the west of the Atlantic Ocean and the Pacific Ocean, as well as parts of the Pacific Ocean, with the magnitude of DRE_{SW} greater than -20 μW m^{-2}, which is direct linked to the spatial distribution of the atmospheric concentration of MPs as illustrated in Fig. 1. Fig. 5B illustrates the DRE_{SW} from the Agricultural sources. The associated DRE is higher in regions with intensive agricultural practices such as the West Africa (up to -81 μW m^{-2}), of the northern India (up to -91 μW m^{-2}), and the East Australia (up to -218 μW m^{-2}). These regions have higher concentrations of MPs from agricultural runoff, plastic mulches, and other farming-related activities. The high DRE calculated in these

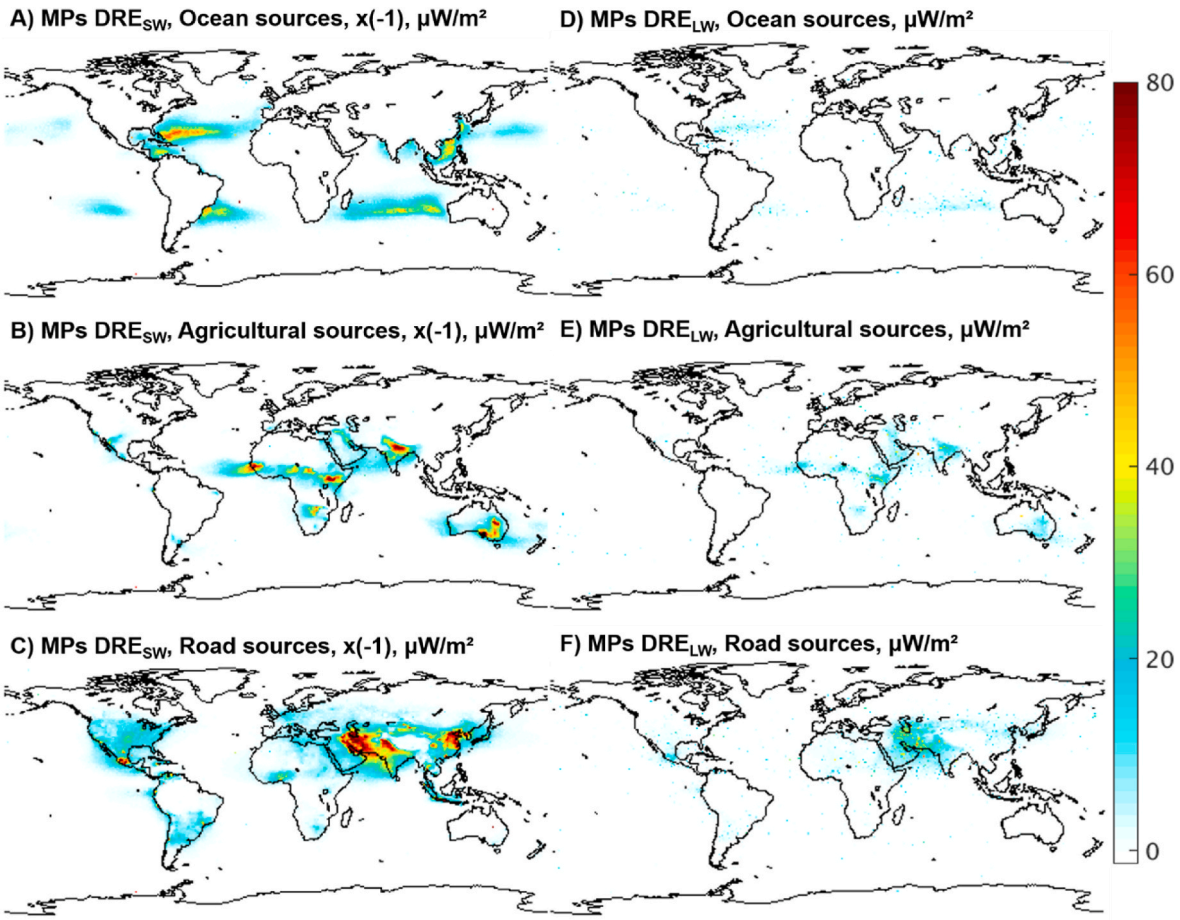

Fig. 5. Annual mean DRE_{SW} of MPs at top of atmosphere from A) Ocean Source, B) Ocean Source, C) Road Source, and DRE_{LW} from D) Ocean Source, E) Ocean Source, F) Road Source.

regions suggests that agricultural MP pollution may exacerbate local and regional climate changes, particularly in areas already experiencing warming trends due to land-use changes and industrialization. The DRE_{SW} from the road sources is most concentrated in urbanized regions and areas with dense road networks, such as Europe, North America, the Middle East, and East Asia. These urbanized areas, with their high levels of traffic and industrial activity, exhibit significant shortwave radiative effect due to the presence of MPs in the atmosphere. i.e. The average DRE_{SW} and DRE_{LW} due to the atmospheric MPs in the North China Plain of the East Asia are -67 μW m^{-2} and 8.1 μW m^{-2}, respectively. The urban heat island effect, already contributing to warming in these areas, could be further exacerbated by the absorption of longwave radiation by road-sourced MPs.

We find that the contributions of different MP sources to DRE_{SW} and DRE_{LW} also vary significantly with altitude. The contribution of ocean-sourced MPs to total DRE_{SW} decreases from 29 % at the top of the atmosphere to 2.6 % at the surface. Meanwhile, the contributions from agricultural and road sources increases significantly with the altitude decreases, which increase from 24.6 % to 38.3 % and from 46.1 % to 60.3 %, respectively. A similar trend is calculated for DRE_{LW}, where the contribution of ocean-sourced MPs drops from 16.7 % to 5.7 % with decreasing altitude. This indicates that the ocean-sourced MPs are a more significant contributor to both shortwave and longwave radiative balance at the top of the atmosphere. Moreover, while ocean-sourced MPs account for 52.6 % of the total MPs suspended in the atmosphere, their smaller contribution to the thermal radiation balance at different altitudes highlights the effects of the lower surface albedo of ocean and the vertical transport limitation of MPs.

Similar significant uncertainties also exist when estimating the contribution of different emission sources to DRE. For example, our estimation of the ocean-sourced MP emission is 171 Gg $year^{-1}$ (Fu et al., 2023). In contrast, Brahney et al. (2021) suggests a much higher ocean-sourced MPs emission of 8600 Gg $year^{-1}$. Meanwhile, Bucci et al. (2024) and Yang et al. (2025) report the ocean-sourced MPs emissions that are one to two orders of magnitudes lower than our model results ($\sim$1.2 and $\sim$10 Gg $year^{-1}$, respectively). These discrepancies may arise from differences in emission and observation data used, as well as factors such as the seasonal variability of emissions and sea-to-air particle transfer limitations. In addition, there may be significant difference between real-world conditions and simulation/theorical estimations. Considering the varying contribution capabilities of different atmospheric MPs emission sources and the impacts of environmental and meteorological conditions, estimating the DRE from different atmospheric MPs emission sources is likely to be more complex and highly uncertain. So, more field observations at different locations worldwide are thus of vital importance to further constrain the emissions and reduce uncertainties. Moreover, conducting multi-model fusion and intercomparison studies in the future could effectively reduce uncertainties stemming from data, model structure and parameter differences. While uncertainties in atmospheric plastic emissions do affect the accuracy of estimating the contribution of different emission sources to DRE, but our results as a first cut in estimating the relative contribution from these sources still make sense. Furthermore, our results indicate that the DRE of atmospheric MPs is not only simply linearly related to plastic emission, but is also affected by surface albedo, water vapor content, and other factors. This insight will be meaningful for guiding future efforts to effectively regulate atmospheric plastic emissions from the perspective of reducing the DRE of atmospheric plastics.

3.5. DRE from MPs with different size bins

We also calculate the DRE of MPs with different size bins due to the unequal size composition of the atmospheric MPs and the significant impact of particle size of MPs on radiative effect. The contributions from different size bins are directly calculated based on the size distribution of atmospheric MPs, not normalized by the mass concentration of each bin. Despite the large uncertainties associated with our estimate of the size distribution of atmospheric MPs, our model results indicate that MPs with different sizes are not equal in contributing DREs. MPs with the size of 15 μm, 35 μm and 70 μm contribute more than 97 % to the total DRE_{SW} and DRE_{LW} from MPs. However, the impact of smaller particles (<7 μm) is less pronounced, likely due to their much smaller concentration in the atmosphere (Fig. S2). Our results suggest that MPs with a size of 35 μm have the largest radiative impact, with the annual mean DRE_{SW} (Fig. 6B) and DRE_{LW} (Fig. 6E) at the top of the atmosphere being -4.83 μW m^{-2} (53.3 % of total DRE_{SW}) and 1.44 μW m^{-2} (52.8 % of total DRE_{SW}), respectively. Meanwhile, the contribution of MPs with the size of 15 μm and 70 μm to DRE_{SW} are 18.1 % and 26.6 % (similar contributions to DRE_{LW}). However, the three size bin s MPs only account for 43.6 % (15 μm), 20.0 % (35 μm) and 2.4 % (70 μm) of total MPs in the atmosphere. These significant disparities between their contributions to concentration and DRE indicate that the DRE of MPs is highly influenced by their size within a certain particle size range, as large MPs have greater DRE magnitudes than small MPs at the same number concentration level. This can be explained by their different optical cross-section constrained by sizes. Although, the proportion of atmospheric MPs with large size is relatively small, their ability to affect radiative fluxes make them cannot be ignored. Meanwhile, abrasion and fragmentation of large-sized-MPs can continue emit small-sized-MPs in the atmosphere. As the emission of atmospheric MPs is keep rising, regulating the emission of large-sized-MPs can effectively reduce the DRE of MPs.

4. Conclusion

In this study, we quantify the direct radiative effects (DRE) of the atmospheric microplastics (MPs) and analyze their spatial distribution, source contribution, and size-dependent impacts. Our findings indicate that the total DRE of MPs is predominantly concentrated in densely populated and arid regions, where high MP emissions and favorable atmospheric conditions allow MPs to exert a stronger radiative influence. These areas experience both shortwave cooling and longwave warming effects from MPs, but the net DRE in these areas is negative, indicating the overall cooling effects of MPs and their potential implications for regional climate dynamics. Despite the high proportion of the ocean-sourced MPs in the total atmospheric MP concentration, their contribution to DRE is relatively low compared to land-based sources. This discrepancy suggests that ocean-sourced MPs may be less optically active or are more likely to remain suspended in lower-impact regions of the atmosphere. Meanwhile, the contribution to DRE from road-sourced MPs is relatively high, which indicates that regulating road plastic emission may be meaningful for reducing atmospheric MPs' DRE. The vertical difference of annual mean net DRE, reveal that MPs exhibit stronger radiative effects with the altitude rising. The vertical differences highlight the complex interactions between MPs and atmospheric radiation and underscore the need for further research into MPs long-range transport and deposition mechanisms. Our study also confirms that MP size plays a key role in determining DRE, with larger MPs exhibiting larger radiative effects when their mass is the same as that of smaller MPs. This is due to their higher efficiency in interacting with radiation per unit mass, which results in increased scattering and absorption capabilities compared to smaller MPs. Consequently, the size distribution of MPs in the atmosphere is a crucial factor in estimating their overall radiative impact.

Although the current DRE of MPs is relatively small compared to the DRE caused by other aerosols, plastic pollution is continuously escalating, and the concentration of airborne MPs will continue to increase. As a result, MPs' radiative effect effects will be enhanced with the projected growth of plastic production and plastic waste, and the atmospheric burden of MPs may become an increasingly significant factor in climate forcing. Additionally, as aerosol concentrations from other sources (e.g., sulfate and black carbon) decrease due to emission

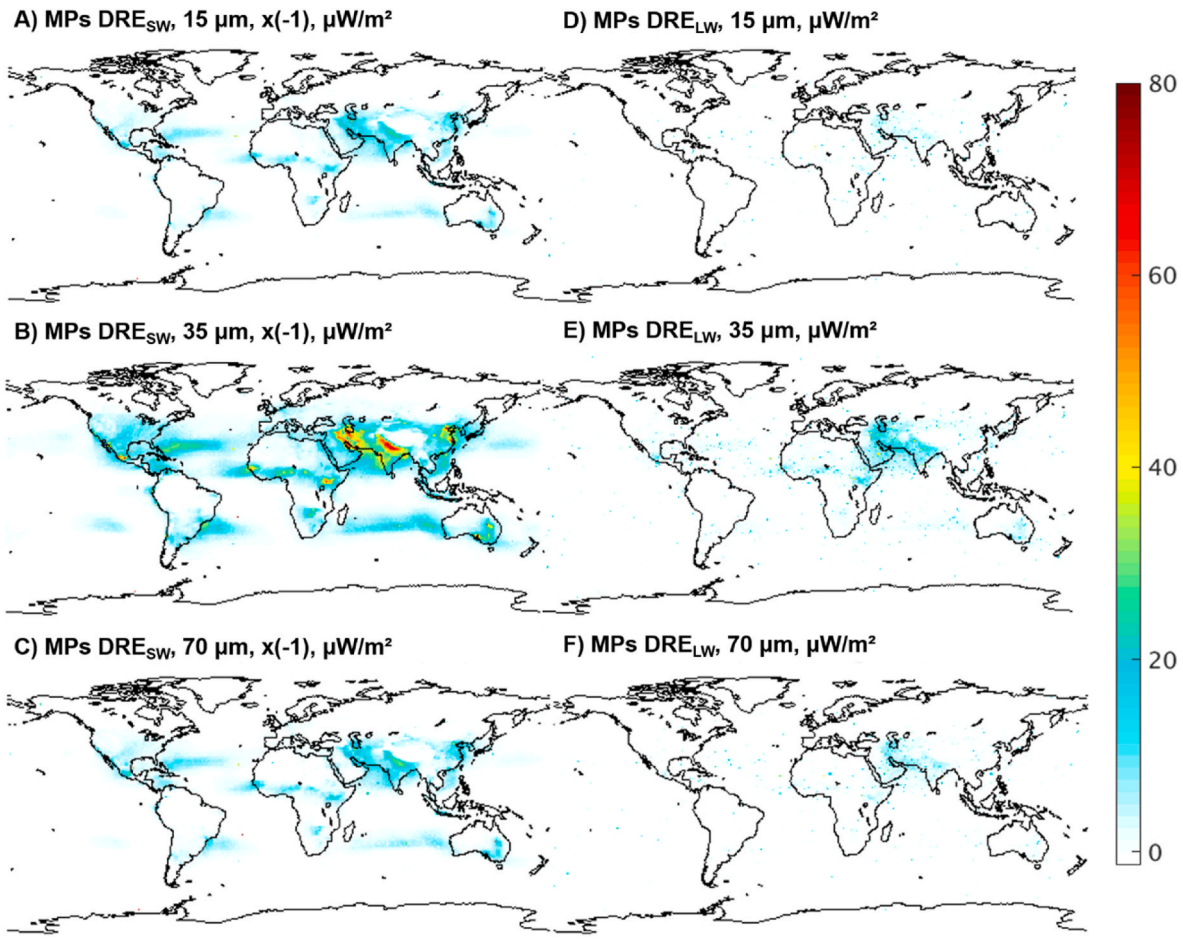

Fig. 6. Annual mean DRE$_{SW}$ of MPs at top of atmosphere with size bin of A) 15 μm, B) 35 μm, C) 70 μm, and DRE$_{LW}$ of MPs with size bin of D) 15 μm, E) 35 μm, F) 70 μm.

reduction policies, the relative importance of MPs in atmospheric radiative effect will grow. The long-term influence of MPs on the Earth's radiation budget may become more pronounced, further reinforcing the need for comprehensive atmospheric monitoring and modeling of MPs' DRE. Finally, we acknowledge that MPs may also exert indirect effects, such as interacting with clouds and other aerosols, which could alter their overall radiative impact (Aeschlimann et al., 2022). For example, MPs may have similar ice nucleating activity to mineral dust under certain temperature range (Busse et al., 2024). Tatsii et al. (2025) find that ice-active MPs can account for more than 40 % of the total INP (ice nucleating particles) number in the tropical. Atmospheric MPs' impacts on climate may be non-negligible after combing their direct (DRE) and indirect impacts (INP). Therefore, future studies should explore these potential synergistic and antagonistic effects to improve our understanding of MPs' impacts on climate. Given the growing urgency of plastic governance and climate policy, understanding the atmospheric role of MPs is essential for developing effective strategies that address both environmental pollution and climate change simultaneously. Our work provides a crucial foundation for future research and policy considerations in this emerging field.

CRediT authorship contribution statement

Qiaotong Pang: Writing – review & editing, Writing – original draft, Visualization, Validation, Software, Investigation, Funding acquisition, Formal analysis, Data curation. **Xuan Wang:** Writing – review & editing, Software, Methodology, Data curation. **Bingliang Zhuang:** Writing – review & editing, Methodology, Data curation, Conceptualization. **Haikun Wang:** Writing – review & editing, Supervision. **Yanxu Zhang:** Writing – review & editing, Visualization, Validation, Supervision, Software, Resources, Project administration, Methodology, Investigation, Funding acquisition, Formal analysis, Data curation, Conceptualization.

Data availability

The GEOS-Chem code is available at https://www.geos-chem.seas.harvard.edu. The GC-MP code and data are available at: https://doi.org/10.17632/52knh3btb3.1. The RRTMG model is available at http://rtweb.aer.com/rrtm_frame.html. Any additional information required to reanalyze the data reported in this paper is available from the lead contact upon request.

Declaration of competing interest

The authors declare that they have no known competing financial interests or personal relationships that could have appeared to influence the work reported in this paper.

Acknowledgments

This study is supported by the National Key R&D Program of China (2019YFA0606803), the Fundamental Research Funds for the Central Universities, China (0207–14380188, 0207–14380168), the "GeoX" Interdisciplinary Research Funds for Frontiers Science Center for Critical Earth Material Cycling, Nanjing University, and the Collaborative

Innovation Center of Climate Change, Jiangsu Province, and the Post-graduate Research & Practice Innovation Program of Jiangsu Province (KYCX23_0125).

Appendix A. Supplementary data

Supplementary data to this article can be found online at https://doi.org/10.1016/j.atmosenv.2025.121305.

Data availability

Data will be made available on request.

References

Aeschlimann, M., Li, G., Kanji, Z.A., Mitrano, D.M., 2022. Potential impacts of atmospheric microplastics and nanoplastics on cloud formation processes. Nat. Geosci. 15 (12), 967–975. https://doi.org/10.1038/s41561-022-01051-9.

Alexander, B., Park, R.J., Jacob, D.J., Li, Q.B., Yantosca, R.M., Savarino, J., Lee, C.C.W., Thiemens, M.H., 2005. Sulfate formation in sea-salt aerosols: constraints from oxygen isotopes. J. Geophys. Res. Atmos. 110 (D10). https://doi.org/10.1029/2004JD005659, 2004JD005659.

Allen, D., Allen, S., Abbasi, S., Baker, A., Bergmann, M., Brahney, J., Butler, T., Duce, R. A., Eckhardt, S., Evangeliou, N., Jickells, T., Kanakidou, M., Kershaw, P., Laj, P., Levermore, J., Li, D., Liss, P., Liu, K., Mahowald, N., et al., 2022. Microplastics and nanoplastics in the marine-atmosphere environment. Nat. Rev. Earth Environ. 3 (6), 393–405. https://doi.org/10.1038/s43017-022-00292-x.

Brahney, J., Mahowald, N., Prank, M., Cornwell, G., Klimont, Z., Matsui, H., Prather, K. A., 2021. Constraining the atmospheric limb of the plastic cycle. Proc. Natl. Acad. Sci. 118 (16), e2020719118. https://doi.org/10.1073/pnas.2020719118.

Bucci, S., Richon, C., Bakels, L., 2024. Exploring the Transport Path of Oceanic Microplastics in the Atmosphere. Environ. Sci. Technol. 58 (32), 14338–14347. https://doi.org/10.1021/acs.est.4c03216.

Busse, H.L., Ariyasena, D.D., Orris, J., Freedman, M.A., 2024. Pristine and aged microplastics can nucleate ice through Immersion Freezing. ACS ES&T Air 1 (12), 1579–1588. https://doi.org/10.1021/acsestair.4c00146.

Chen, Q., Shi, G., Revell, L.E., Zhang, J., Zuo, C., Wang, D., Le Ru, E.C., Wu, G., Mitrano, D.M., 2023. Long-range atmospheric transport of microplastics across the southern hemisphere. Nat. Commun. 14 (1), 7898. https://doi.org/10.1038/s41467-023-43695-0.

Clough, S.A., Shephard, M.W., Mlawer, E.J., Delamere, J.S., Iacono, M.J., Cady-Pereira, K., Boukabara, S., Brown, P.D., 2005. Atmospheric radiative transfer modeling: a summary of the AER codes. J. Quant. Spectrosc. Radiat. Transf. 91 (2), 233–244. https://doi.org/10.1016/j.jqsrt.2004.05.058.

Cózar, A., Echevarría, F., González-Gordillo, J.I., Irigoien, X., Úbeda, B., Hernández-León, S., Palma, Á.T., Navarro, S., García-de-Lomas, J., Ruiz, A., Fernández-de-Puelles, M.L., Duarte, C.M., 2014. Plastic debris in the open ocean. Proc. Natl. Acad. Sci. 111 (28), 10239–10244. https://doi.org/10.1073/pnas.1314705111.

Duncan Fairlie, T., Jacob, D.J., Park, R.J., 2007. The impact of transpacific transport of mineral dust in the United States. Atmos. Environ. 41 (6), 1251–1266. https://doi.org/10.1016/j.atmosenv.2006.09.048.

Evangeliou, N., Grythe, H., Klimont, Z., Heyes, C., Eckhardt, S., Lopez-Aparicio, S., Stohl, A., 2020. Atmospheric transport is a major pathway of microplastics to remote regions. Nat. Commun. 11 (1), 3381. https://doi.org/10.1038/s41467-020-17201-9.

Evangeliou, N., Tichý, O., Eckhardt, S., Zwaaftink, C.G., Brahney, J., 2022. Sources and fate of atmospheric microplastics revealed from inverse and dispersion modelling: from global emissions to deposition. J. Hazard Mater. 432, 128585. https://doi.org/10.1016/j.jhazmat.2022.128585.

Fu, Y., Pang, Q., Suo, Lang Zhuo Ga, Wu, P., Wang, Y., Mao, M., Yuan, Z., Xu, X., Liu, K., Wang, X., Li, D., Zhang, Y., 2023. Modeling atmospheric microplastic cycle by GEOS-Chem: an optimized estimation by a global dataset suggests likely 50 times lower ocean emissions. One Earth 6 (6), 705–714. https://doi.org/10.1016/j.oneear.2023.05.012.

Global plastic production share by region 2023, 2024. Statista. https://www.statista.com/statistics/281126/global-plastics-production-share-of-various-countries-and-regions/.

Heald, C.L., Ridley, D.A., Kroll, J.H., Barrett, S.R.H., Cady-Pereira, K.E., Alvarado, M.J., Holmes, C.D., 2014. Contrasting the direct radiative effect and direct radiative forcing of aerosols. Atmos. Chem. Phys. 14 (11), 5513–5527. https://doi.org/10.5194/acp-14-5513-2014.

Huang, Y., Kok, J.F., Saito, M., Muñoz, O., 2023. Single-scattering properties of ellipsoidal dust aerosols constrained by measured dust shape distributions. Atmos. Chem. Phys. 23 (4), 2557–2577. https://doi.org/10.5194/acp-23-2557-2023.

Jaeglé, L., Quinn, P.K., Bates, T.S., Alexander, B., Lin, J.-T., 2011. Global distribution of sea salt aerosols: New constraints from in situ and remote sensing observations. Atmos. Chem. Phys. 11 (7), 3137–3157. https://doi.org/10.5194/acp-11-3137-2011.

Leresche, F., Salazar, J.R., Pfotenhauer, D.J., Hannigan, M.P., Majestic, B.J., Rosario-Ortiz, F.L., 2021. Photochemical aging of atmospheric particulate matter in the aqueous phase. Environ. Sci. Technol. https://doi.org/10.1021/acs.est.1c00978 acs.est.1c00978.

Lin, S., B Rood, R., 1996. Multidimensional flux-form semi-Lagrangian transport schemes. Mon. Weather Rev. 124, 2046–2070.

Liu, H., Jacob, D.J., Bey, I., Yantosca, R.M., 2001. Constraints from ^{210}Pb and ^{7}Be on wet deposition and transport in a global three-dimensional chemical tracer model driven by assimilated meteorological fields. J. Geophys. Res. Atmos. 106 (D11), 12109–12128. https://doi.org/10.1029/2000JD900839.

Long, X., Fu, T.-M., Yang, X., Tang, Y., Zheng, Y., Zhu, L., Shen, H., Ye, J., Wang, C., Wang, T., Li, B., 2022. Efficient atmospheric transport of microplastics over Asia and adjacent oceans. Environ. Sci. Technol. 56 (10), 6243–6252. https://doi.org/10.1021/acs.est.1c07825.

Luo, D., Chu, X., Wu, Y., Wang, Z., Liao, Z., Ji, X., Ju, J., Yang, B., Chen, Z., Dahlgren, R., Zhang, M., Shang, X., 2024. Micro- and nano-plastics in the atmosphere: a review of occurrence, properties and human health risks. J. Hazard Mater. 465, 133412. https://doi.org/10.1016/j.jhazmat.2023.133412.

Morioka, T., Tanaka, S., Kohama-Inoue, A., Watanabe, A., 2024. The quantification of the airborne plastic particles of 0.43–11 μm: procedure development and application to atmospheric environment. Chemosphere 351, 141131. https://doi.org/10.1016/j.chemosphere.2024.141131.

Revell, L.E., Kuma, P., Le Ru, E.C., Somerville, W.R.C., Gaw, S., 2021. Direct radiative effects of airborne microplastics. Nature 598 (7881), 462–467. https://doi.org/10.1038/s41586-021-03864-x.

Schaaf, C.B., Gao, F., Strahler, A.H., Lucht, W., Li, X., Tsang, T., Strugnell, N.C., Zhang, X., Jin, Y., Muller, J.-P., Lewis, P., Barnsley, M., Hobson, P., Disney, M., Roberts, G., Dunderdale, M., Doll, C., d'Entremont, R.P., Hu, B., et al., 2002. First operational BRDF, albedo nadir reflectance products from MODIS. Rem. Sens. Environ. 83 (1–2), 135–148. https://doi.org/10.1016/S0034-4257(02)00091-3.

Tatsii, D., Gasparini, B., Evangelou, I., Bucci, S., Stohl, A., 2025. Do microplastics contribute to the total number concentration of ice nucleating particles? J. Geophys. Res. Atmos. 130 (2), e2024JD042827. https://doi.org/10.1029/2024JD042827.

Wang, Q., Jacob, D.J., Fisher, J.A., Mao, J., Leibensperger, E.M., Carouge, C.C., Le Sager, P., Kondo, Y., Jimenez, J.L., Cubison, M.J., Doherty, S.J., 2011. Sources of carbonaceous aerosols and deposited black carbon in the Arctic in winter-spring: implications for radiative forcing. Atmos. Chem. Phys. 11 (23), 12453–12473. https://doi.org/10.5194/acp-11-12453-2011.

Wang, X., Zhai, S., Shen, L., 2024. Cooling from aerosol–radiation interaction of anthropogenic coarse particles in China. Npj Clim. Atmos. Sci. 7 (1), 220. https://doi.org/10.1038/s41612-024-00773-4.

World steel in Figures 2022—worldsteel.org. https://worldsteel.org/data/world-steel-in-figures-2022/, 2023.

Wu, W., 2004. Depth-averaged two-dimensional numerical modeling of unsteady flow and nonuniform sediment transport in open channels. J. Hydraul. Eng. 130 (10), 1013–1024. https://doi.org/10.1061/(ASCE)0733-9429(2004)130:10(1013).

Xu, Y., Ou, Q., Van Der Hoek, J.P., Liu, G., Lompe, K.M., 2024. Photo-oxidation of micro- and nanoplastics: physical, chemical, and biological effects in environments. Environ. Sci. Technol. 58 (2), 991–1009. https://doi.org/10.1021/acs.est.3c07035.

Yang, S., Brasseur, G., Walters, S., Lichtig, P., Li, C.W.Y., 2025. Global atmospheric distribution of microplastics with evidence of low oceanic emissions. npj Clim. Atmos. Sci. 8 (1), 81. https://doi.org/10.1038/s41612-025-00914-3.

Yang, H., Xue, Y., Sha, X., Yang, J., Wang, X., Suvdantsetseg, B., Kuroda, K., Pu, J., Wang, L., 2024. Influence of regional environmental variables on the radiative forcing of atmospheric microplastics. Eco-Environ. Health. https://doi.org/10.1016/j.eehl.2024.11.002. S277298502400070X.

Zhang, X., Qiu, J., Zhao, J., Li, X., Liu, L., 2020. Complex refractive indices measurements of polymers in infrared bands. J. Quant. Spectrosc. Radiat. Transf. 252, 107063. https://doi.org/10.1016/j.jqsrt.2020.107063.

Zhang, Y., Wu, P., Xu, R., Wang, X., Lei, L., Schartup, A.T., Peng, Y., Pang, Q., Wang, X., Mai, L., Wang, R., Liu, H., Wang, X., Luijendijk, A., Chassignet, E., Xu, X., Shen, H., Zheng, S., Zeng, E.Y., 2023. Plastic waste discharge to the global ocean constrained by seawater observations. Nat. Commun. 14 (1), 1372. https://doi.org/10.1038/s41467-023-37108-5.

Zhao, X., Wang, J., Yee Leung, K.M., Wu, F., 2022. Color: an important but overlooked factor for plastic photoaging and microplastic formation. Environ. Sci. Technol. 56 (13), 9161–9163. https://doi.org/10.1021/acs.est.2c02402.

Zhu, X., Huang, W., Fang, M., Liao, Z., Wang, Y., Xu, L., Mu, Q., Shi, C., Lu, C., Deng, H., Dahlgren, R., Shang, X., 2021. Airborne microplastic concentrations in five megacities of northern and Southeast China. Environ. Sci. Technol. https://doi.org/10.1021/acs.est.1c03618 acs.est.1c03618.